scientific reports

Check for updates

OPEN

Twisted space-frequency and space-time partially coherent beams

Milo W. Hyde IV

We present partially coherent sources that are statistically twisted in the space-frequency and space-time domains. Beginning with the superposition rule for genuine partially coherent sources, we derive source plane expressions for the cross-spectral density (CSD) and mutual coherence functions (MCFs) for twisted space-frequency and space-time Gaussian Schell-model (GSM) beams. Using the Fresnel approximation to the free-space Green's function, we then paraxially propagate the CSD and MCF to any plane $z > 0$. We discuss the beams' behavior as they propagate, with particular emphasis on how the beam shape rotates or tumbles versus z. To validate our analysis, we simulate the generation and subsequent propagation of twisted space-frequency and space-time GSM beams. We compare the simulated moments to the corresponding theoretical predictions and find them to be in excellent agreement. Lastly, we describe how to physically synthesize twisted space-frequency and space-time partially coherent sources.

Approximately 30 years ago, Allen et al. discovered that fields with a vortex wavefront, e.g., Laguerre–Gaussian beams, carried orbital angular momentum (OAM)[1,2]. This initial discovery has spawned much research in applying vortex beams in free-space optical communications, optical tweezers, astronomy, etcetera[3–8].

In 1993, Simon and Mukunda introduced the concept of a twisted partially coherent field[9]. Like fields with vortex phase fronts, twisted partially coherent beams carry OAM. They differ from traditional vortex fields in that the twist, or rotation is statistical in nature and exists only in the context of stochastic beams, i.e., the twist disappears in the coherent limit. Like Allen et al.'s seminal OAM work, Simon and Mukunda's twisted partially coherent beams have generated significant interest in the intervening years[10–21].

A vast majority of the references pertaining to vortex or twisted beams, whether they be fully coherent or stochastic, deal with spatial vortices or twists in the plane orthogonal to the direction of propagation, e.g., the x–y plane for a z propagating wave. All of these beams possess OAM orientated in the longitudinal direction. Recently, a class of vortex beams has been introduced where the vortex exists in the space-time domain[22–27]. Referred to as spatiotemporal optical vortices (STOVs), these beams carry transverse OAM. Their study and subsequent synthesis opens up the possibility for novel uses in optical manipulation, optical tweezing, and other applications.

Motivated by the existence of STOVs and their potential applications, we introduce the space-frequency and space-time extensions of Simon and Mukunda's spatially twisted partially coherent beams. Analogous to the relationship between spatial and spatiotemporal vortices, twisted space-frequency and space-time partially coherent sources possess statistical twists between their spatial and temporal dimensions. Like STOVs, these beams carry transverse OAM, and, in addition, rotate or tumble as they propagate.

We emphasize two foundational papers that describe spatiotemporal coupling which are germane to our work. The first is a paper by Akturk et al. that develops a general mathematical theory for spatiotemporal coupling of coherent Gaussian pulsed beams[28]. The second is authored by Wang et al. and presents a 6×6 matrix formalism which describes the behavior of partially coherent Gaussian Schell-model (GSM) pulsed beams in linear, dispersive media[29]. Although spatiotemporal coupling has been researched in the past by these and numerous other authors, no one, to our knowledge, has formally presented—mathematically and physically described the propagation behaviors, or generated random field realizations of—twisted space-frequency and space-time partially coherent sources, as we do here.

In the next section, we derive expressions for the cross-spectral density (CSD) and mutual coherence functions (MCFs) for twisted space-frequency and space-time partially coherent beams, respectively. Assuming sources of GSM form[30,31], we study the behaviors of twisted space-frequency and space-time beams as they

Air Force Institute of Technology, Dayton, OH 45433, USA. email: milo.hyde@us.af.mil

propagate in free space by evaluating the CSD and MCF paraxial propagation integrals. We simulate the synthesis and propagation of these beams, and compare the simulated, or sample statistical moments to their corresponding theoretical expressions to validate our analysis. We conclude with a discussion of how to physically synthesize these new partially coherent beams and a summary of our work.

Methods

In this section, we theoretically introduce twisted space-frequency and space-time partially coherent sources.

Twisted space-frequency partially coherent sources. Our analysis begins with the necessary and sufficient criterion for a genuine CSD function[32,33]:

$$W(x_1,x_2,\omega_1,\omega_2)=\iint_{-\infty}^{\infty}p(\nu_x,\nu_\omega)H(x_1,\omega_1;\nu_x,\nu_\omega)H^*(x_2,\omega_2;\nu_x,\nu_\omega)\mathrm{d}\nu_x\mathrm{d}\nu_\omega, \tag{1}$$

where ω is the radian frequency, p is any positive function, and H is an arbitrary kernel. Equation (1) is also referred to as the superposition rule in the literature. For simplicity, we restrict our analysis to one spatial dimension x.

Adapting Mei and Korotkova's[14] twist kernel, we let H be

$$\begin{aligned}H(x,\omega;\nu_x,\nu_\omega)=&H(x,\omega;\nu_x)H(x,\omega;\nu_\omega)\\ H(x,\omega;\nu_x)=&\exp\left(-\frac{\sigma_x}{2}x^2\right)\exp\left(-\frac{\sigma_\omega}{2}\bar{\omega}^2\right)\exp\left[-\mathrm{j}\left(x-\mathrm{j}\alpha\mu\omega\right)\nu_x\right]\\ H(x,\omega;\nu_\omega)=&\exp\left(-\frac{\sigma_x}{2}x^2\right)\exp\left(-\frac{\sigma_\omega}{2}\bar{\omega}^2\right)\exp\left[-\mathrm{j}\left(\omega-\mathrm{j}\beta\mu x\right)\nu_\omega\right],\end{aligned} \tag{2}$$

where $\bar{\omega}=\omega-\omega_c$ and ω_c is the radian frequency of the light, or carrier wave. We will discuss σ_x, σ_ω, α, β, and μ later on in the paper. We note that other twist kernels exist in the literature[10,15,18,19,21] and can be adapted in a similar manner as above to produce twisted space-frequency and space-time beams.

To generate twisted GSM beams, we choose p to be[10,14,15,18,19,21]

$$p(\nu_x,\nu_\omega)=p(\nu_x)p(\nu_\omega)=\sqrt{\frac{\alpha}{\pi}}\exp\left(-\alpha\nu_x^2\right)\sqrt{\frac{\beta}{\pi}}\exp\left(-\beta\nu_\omega^2\right). \tag{3}$$

Like H in Eq. (2), other p can be used, e.g., the multi-Gaussian p in Refs.[14,34]. Substituting Eqs. (2) and (3) into (1) and evaluating the integrals yields a CSD of the form

$$\begin{aligned}W(x_1,x_2,\omega_1,\omega_2)=&\exp\left(-\frac{x_1^2+x_2^2}{4W_x^2}\right)\exp\left[-\frac{(x_1-x_2)^2}{2\delta_x^2}\right]\\ &\times\exp\left(-\frac{\bar{\omega}_1^2+\bar{\omega}_2^2}{4W_\omega^2}\right)\exp\left[-\frac{(\bar{\omega}_1-\bar{\omega}_2)^2}{2\delta_\omega^2}\right]\exp\left[\mathrm{j}\mu(x_1\bar{\omega}_2-x_2\bar{\omega}_1)\right],\end{aligned} \tag{4}$$

where W_x and W_ω are the beam and spectral pulse widths, δ_x and δ_ω are the spatial coherence and spectral coherence widths, and μ is the twist parameter. These beam parameters are not independent and are linked in a complex, nonlinear way. Referring back to Eq. (2),

$$\begin{aligned}\frac{1}{4W_x^2}&=\sigma_x-\frac{\beta\mu^2}{2} & \frac{1}{4W_\omega^2}&=\sigma_\omega-\frac{\alpha\mu^2}{2}\\ \frac{1}{2\delta_x^2}&=\frac{1}{4\alpha}+\frac{\beta\mu^2}{4} & \frac{1}{2\delta_\omega^2}&=\frac{1}{4\beta}+\frac{\alpha\mu^2}{4}.\end{aligned} \tag{5}$$

In addition, $|\mu|\delta_x\delta_\omega\le 1$[31,35,36], and therefore, the space-frequency twist necessarily disappears in the coherent limit $\delta_x,\delta_\omega\to\infty$.

Equation (4) has the same basic form as a spatially twisted GSM beam[9,10,12,14,37]; however, here, space and frequency are statistically twisted. It is well known that the spectral density of a spatially twisted stochastic source rotates as the beam propagates. This rotation is in the plane orthogonal to the propagation direction, e.g., x–y plane for a z propagating wave. Twisted space-frequency beams also rotate—this time, in the x–ω plane.

The paraxial, twisted space-frequency GSM CSD at any propagation plane $z>0$ can be found using the two-frequency Fresnel integral, namely,

$$\begin{aligned}W(x_1,x_2,\omega_1,\omega_2,z)=&\frac{\exp\left[\mathrm{j}(k_1-k_2)z\right]\exp\left[\frac{\mathrm{j}}{2z}\left(k_1x_2^2-k_2x_2^2\right)\right]}{z\sqrt{\lambda_1\lambda_2}}\\ &\times\iint_{-\infty}^{\infty}W\left(x_1',x_2',\omega_1,\omega_2\right)\exp\left[\frac{\mathrm{j}}{2z}\left(k_1x_2'^2-k_2x_2'^2\right)\right]\\ &\times\exp\left[-\frac{\mathrm{j}}{z}\left(k_1x_1x_1'-k_2x_2x_2'\right)\right]\mathrm{d}x_1'\mathrm{d}x_2',\end{aligned} \tag{6}$$

where $k_{1,2} = \omega_{1,2}/c$ and $\lambda_{1,2} = 2\pi/k_{1,2}$ are the wavenumbers and wavelengths associated with ω_1 and ω_2, respectively and c is the speed of light. Substituting in Eq. (4) and after much calculus and algebra,

$$\begin{aligned} W(x_1, x_2, \omega_1, \omega_2, z) =& \frac{\sqrt{k_1 k_2}}{2z\Omega} \exp\left[\mathrm{j}(k_1 - k_2)z\right] \exp\left(-\frac{\bar{\omega}_1^2 + \bar{\omega}_2^2}{4W_\omega^2}\right) \exp\left[-\frac{(\bar{\omega}_1 - \bar{\omega}_2)^2}{2\delta_\omega^2}\right] \\ & \times \exp\left[\frac{\mathrm{j}\mu^2}{8z\Omega^2}\left(k_1\bar{\omega}_1^2 - k_2\bar{\omega}_2^2\right)\right] \exp\left[\frac{\mathrm{j}}{2z}\left(1 - \frac{k_1 k_2}{4z^2\Omega^2}\right)\left(k_1 x_1^2 - k_2 x_2^2\right)\right] \\ & \times \exp\left[-\frac{(\mu\bar{\omega}_1 - k_2 x_2/z)^2 + (\mu\bar{\omega}_2 - k_1 x_1/z)^2}{16W_x^2\Omega^2}\right] \\ & \times \exp\left\{-\frac{\left[(\mu\bar{\omega}_1 - k_2 x_2/z) - (\mu\bar{\omega}_2 - k_1 x_1/z)\right]^2}{8\delta_x^2\Omega^2}\right\} \\ & \times \exp\left[\mathrm{j}\mu\frac{k_1 k_2}{4z^2\Omega^2}(x_1\bar{\omega}_2 - x_2\bar{\omega}_1)\right], \end{aligned} \tag{7}$$

where $\Omega^2 = \left[\sigma - \mathrm{j}k_1/(2z)\right]\left[\sigma + \mathrm{j}k_2/(2z)\right] - \left[1/\left(2\delta_x^2\right)\right]^2$ and $\sigma = 1/\left(4W_x^2\right) + 1/\left(2\delta_x^2\right)$.

The exponentials on the third, fourth, and fifth lines of Eq. (7) correspond to the beam shape, coherence, and twist, respectively. Because of the initial space-frequency coupling, the spectral content of the beam affects its spatial distribution and equivalently, vice versa.

The spectral density S of the source can be found by evaluating Eq. (7) at the same space and frequency points[30,31], i.e.,

$$\begin{aligned} S(x, \omega, z) =& W(x, x, \omega, \omega, z) \\ =& \frac{N_F}{\sqrt{1 + 4\gamma_x^2 + N_F^2}} \exp\left[-\left(1 + \mu^2\frac{4W_x^2 W_\omega^2}{1 + 4\gamma_x^2 + N_F^2}\right)\frac{\bar{\omega}^2}{2W_\omega^2}\right] \\ & \times \exp\left[-\left(\frac{N_F^2}{1 + 4\gamma_x^2 + N_F^2}\right)\frac{x^2}{2W_x^2}\right] \exp\left(\mu\frac{2N_F}{1 + 4\gamma_x^2 + N_F^2}\bar{\omega}x\right), \end{aligned} \tag{8}$$

where $\gamma_x^2 = W_x^2/\delta_x^2$ and $N_F = 2kW_x^2/z$ is the coherent Gaussian beam Fresnel number. In order, the exponentials in Eq. (8) physically correspond to the spectral beam shape, spatial beam shape, and x-ω plane rotation. We note that the coefficient in the spectral beam shape exponential is greater than or equal to one. This, when combined with the fact that the spatial beam shape is only affected by diffraction (depends on Fresnel number, spatial beam size, and coherence radius), means that the beam essentially "trades" spectrum to rotate. As $z \to \infty$ or $N_F \to 0$, the spectral beam radius asymptotes (the spectral beam shape does not appreciably change), diffraction dominates, and the beam no longer rotates.

Although evident from the numerous references describing rotating coherent beams[28,37–39], it is important to point out that beam rotation does not imply partial coherence. Rotation, therefore, is a characteristic of partially coherent twisted beams, not a defining characteristic.

Twisted space-time partially coherent sources. Similar to the approach we used above to produce twisted space-frequency sources, we can also construct twisted space-time partially coherence sources. In many respects, these sources are more physically intuitive than their twisted space-frequency counterparts, as the rotation occurs in the x–t plane. Paraxially, t is closely related to the propagation direction z, and therefore, these beams rotate or tumble as the beam propagates.

Like above, we begin with the superposition rule, this time for the MCF Γ[32,33]:

$$\Gamma(x_1, x_2, t_1, t_2) = \int_{-\infty}^{\infty} p(\nu_x) H(x_1, t_1; \nu_x) H^*(x_2, t_2; \nu_x) \mathrm{d}\nu_x \int_{-\infty}^{\infty} p(\nu_t) H(x_1, t_1; \nu_t) H^*(x_2, t_2; \nu_t) \mathrm{d}\nu_t, \tag{9}$$

where p and H are

$$\begin{aligned} p(\nu_x, \nu_t) &= p(\nu_x)p(\nu_t) = \sqrt{\frac{\alpha}{\pi}} \exp\left(-\alpha\nu_x^2\right)\sqrt{\frac{\beta}{\pi}} \exp\left(-\beta\nu_t^2\right) \\ H(x, t; \nu_x, \nu_t) &= H(x, t; \nu_x)H(x, t; \nu_t) \\ H(x, t; \nu_x) &= \exp\left(-\frac{\sigma_x}{2}x^2\right) \exp\left(-\frac{\sigma_t}{2}t^2\right) \exp\left(-\mathrm{j}\frac{\omega_c}{2}t\right) \exp\left[-\mathrm{j}\left(x - \mathrm{j}\alpha\mu t\right)\nu_x\right] \\ H(x, t; \nu_t) &= \exp\left(-\frac{\sigma_x}{2}x^2\right) \exp\left(-\frac{\sigma_t}{2}t^2\right) \exp\left(-\mathrm{j}\frac{\omega_c}{2}t\right) \exp\left[-\mathrm{j}\left(t - \mathrm{j}\beta\mu x\right)\nu_t\right]. \end{aligned} \tag{10}$$

Substituting the above p and H into Eq. (9) and evaluating the integrals produces an MCF of the form

$$\begin{aligned}\Gamma(x_1,x_2,t_1,t_2) =& \exp\left(-\frac{x_1^2+x_2^2}{4W_x^2}\right)\exp\left[-\frac{(x_1-x_2)^2}{2\delta_x^2}\right]\exp\left[-\mathrm{j}\omega_c(t_1-t_2)\right]\\ &\times\exp\left(-\frac{t_1^2+t_2^2}{4W_t^2}\right)\exp\left[-\frac{(t_1-t_2)^2}{2\delta_t^2}\right]\exp\left[\mathrm{j}\mu(x_1t_2-x_2t_1)\right].\end{aligned} \tag{11}$$

The physical source parameters W_x, W_t, δ_x, δ_t, and μ are related to σ_x, σ_t, α, and β in the same way as the corresponding twisted space-frequency beam parameters—see Eq. (5). As expected, when $\mu = 0$, Eq. (11) simplifies to a traditional GSM pulsed beam[29,40–44].

We can propagate the MCF in Eq. (11) to any plane $z > 0$ using the following integral expression:

$$\Gamma(x_1,x_2,t_1,t_2,z) = \frac{1}{\lambda_c z}\iint_{-\infty}^{\infty}\Gamma\left[x_1',x_2',t_1-\frac{z}{c}-\frac{(x_1-x_1')^2}{2cz},t_2-\frac{z}{c}-\frac{(x_2-x_2')^2}{2cz}\right]\mathrm{d}x_1'\mathrm{d}x_2'. \tag{12}$$

This relation is accurate in the paraxial regime, and if the source is narrowband, i.e., $\omega_c \gg \max(1/W_t, 1/\delta_t)$. Substituting Eqs. (11) into (12) and neglecting terms greater than second order produces

$$\begin{aligned}\Gamma(x_1,x_2,t_1,t_2,z) \approx& \frac{k_c}{2z\Omega}\exp\left[-\mathrm{j}\omega_c(\bar{t}_1-\bar{t}_2)\right]\exp\left(-\frac{\bar{t}_1^2+\bar{t}_2^2}{4W_t^2}\right)\exp\left[-\frac{(\bar{t}_1-\bar{t}_2)^2}{2\delta_t^2}\right]\\ &\times\exp\left[\frac{\mathrm{j}k_c\mu^2}{8z\Omega^2}(\bar{t}_1^2-\bar{t}_2^2)\right]\exp\left[-\frac{\mathrm{j}k_c^3}{8z^3\Omega^2}(x_1^2-x_2^2)\right]\\ &\times\exp\left[-\frac{(\mu\bar{t}_1-k_cx_2/z)^2+(\mu\bar{t}_2-k_cx_1/z)^2}{16W_x^2\Omega^2}\right]\\ &\times\exp\left\{-\frac{\left[(\mu\bar{t}_1-k_cx_2/z)-(\mu\bar{t}_2-k_cx_1/z)\right]^2}{8\delta_x^2\Omega^2}\right\}\\ &\times\exp\left[\mathrm{j}\mu\frac{k_c^2}{4z^2\Omega^2}(x_1\bar{t}_2-x_2\bar{t}_1)\right],\end{aligned} \tag{13}$$

where $\bar{t}_{1,2} = t_{1,2} - z/c - x_{1,2}^2/(2cz)$,

$$\Omega^2 = \left(\frac{1}{4W_x^2}\right)^2(1+4\gamma_x^2+N_F^2), \tag{14}$$

and $N_F = 2k_cW_x^2/z$ is the Fresnel number at the carrier frequency.

Like the spectral density above, the time-varying, ensemble-averaged intensity can be determined by evaluating the MCF at equal space and time points:

$$\begin{aligned}I(x,t,z) =& \Gamma(x,x,t,t,z)\\ =& \frac{N_F}{\sqrt{1+4\gamma_x^2+N_F^2}}\exp\left[-\left(1+\mu^2\frac{4W_x^2W_t^2}{1+4\gamma_x^2+N_F^2}\right)\frac{\bar{t}^2}{2W_t^2}\right]\\ &\times\exp\left[-\left(\frac{N_F^2}{1+4\gamma_x^2+N_F^2}\right)\frac{x^2}{2W_x^2}\right]\exp\left(\mu\frac{2N_F}{1+4\gamma_x^2+N_F^2}\bar{t}x\right).\end{aligned} \tag{15}$$

The behavior of this beam in the x-t plane is the same as that described for the twisted space-frequency GSM source in the x-ω plane.

As briefly stated above, the time t paraxially corresponds to the physical propagation dimension z (i.e., $\bar{t} \approx t - z/c$). As such, when $\mu \neq 0$, a twisted space-time beam tumbles as it propagates, and like beams with STOVs[23,25–27], has a component of OAM in the $\pm y$ direction depending on the sign of μ. Figure 1 and the corresponding Supplementary Video V1 show this behavior for an example twisted space-time GSM partially coherent beam.

Results and discussion

In this section, we simulate the generation of twisted space-frequency and space-time GSM beams. First, we discuss the details of the wave-optics simulations.

Simulation setup. For these simulations, we used computational grids that were 512 points per side. The grid spacings were approximately $\Delta x = 26.9\,\mu$m and $\Delta\omega = 1.11$ GHz in the x and ω dimensions for the space-frequency source, and $\Delta x = 26.9\,\mu$m and $\Delta t = 1.11$ ps in the x and t dimensions for the space-time source.

To generate twisted space-frequency and space-time GSM field realizations, we used their respective superposition rules in Eqs. (1) and (9) as detailed in Ref.[45]. For the paper's completeness and the reader's convenience, we briefly review this synthesis method using the space-time GSM source as an example.

A stochastic instance of a space-time GSM partially coherent source can be generated by evaluating the following integral:

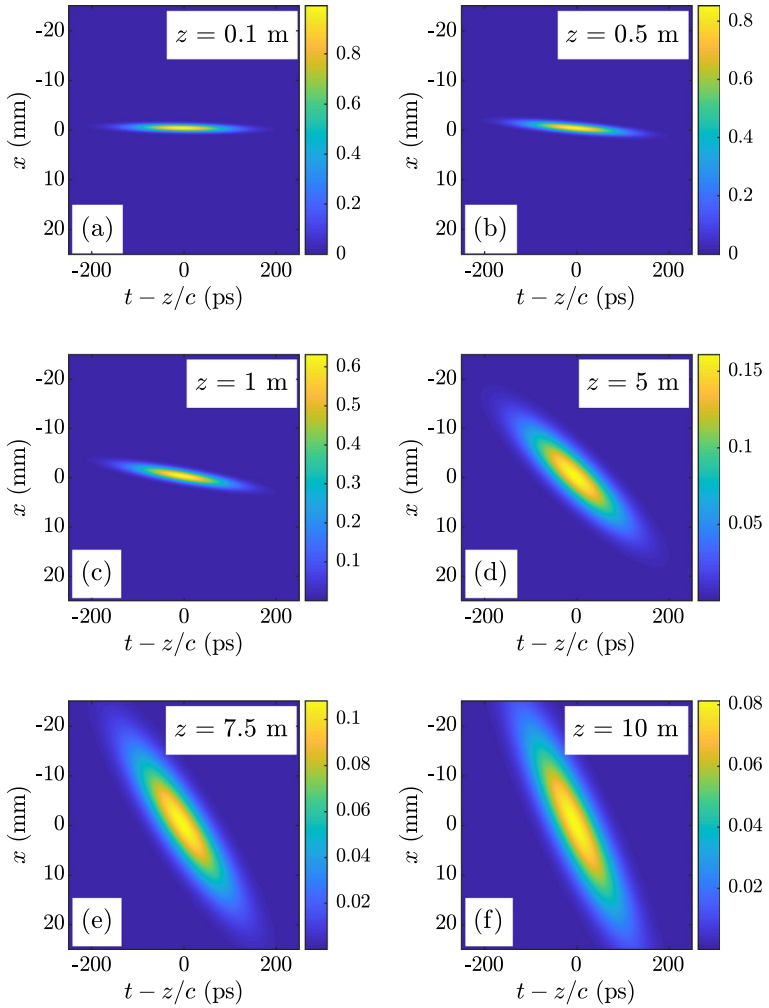

Figure 1. Mean intensity $I(x,t,z)$ for a twisted space-time GSM partially coherent source with $\lambda_c = 1\ \mu$m, $W_x = 0.5$ mm, $\delta_x = 0.27$ mm, $W_t = 70.7$ ps, $\delta_t = 33.3$ ps, and $\mu = 0.1\ (\text{mm ps})^{-1}$—(**a**) $z = 0.1$ m, (**b**) $z = 0.5$ m, (**c**) $z = 1$ m, (**d**) $z = 5$ m, (**e**) $z = 7.5$ m, and (**f**) $z = 10$ m.

$$U(x,t) = \iint_{-\infty}^{\infty} r(v_x, v_t)\left[\frac{1}{2}p(v_x, v_t)\right]^{1/2} H(x,t;v_x,v_t)\mathrm{d}v_x\mathrm{d}v_t, \tag{16}$$

where p and H are given in Eq. (10) and r is a complex, delta-correlated, Gaussian-distributed stochastic function[45]. Taking the autocorrelation of Eq. (16) and noting that $\langle r(v_{x1}, v_{t1})r^*(v_{x2}, v_{t2})\rangle = 2\delta(v_{x1} - v_{x2}, v_{t1} - v_{t2})$ reproduces the space–time source superposition rule given in Eq. (9).

We now express Eq. (16) in discrete form as the integrals are evaluated numerically. In addition, p and H are separable in v_x and v_t. Because of this, we can express the four-dimensional kernel H as the product of two three-dimensional kernels. This results in significant savings in computer memory. We therefore express Eq. (16) as the Hadamard product of two matrix-vector products:

$$\boldsymbol{U}[ij] = \underline{\mathbf{H}}[ij,m]\left\{\boldsymbol{r}[m]\odot\sqrt{\boldsymbol{p}[m]}\right\}\sqrt{\frac{\Delta v_x}{2}}\odot\underline{\mathbf{H}}[ij,n]\left\{\boldsymbol{r}[n]\odot\sqrt{\boldsymbol{p}[n]}\right\}\sqrt{\frac{\Delta v_t}{2}}, \tag{17}$$

where m, n are the discrete v_x, v_t indices, $\Delta v_x, \Delta v_t$ are the spacings in the v_x, v_t dimensions, and ij is a double index corresponding to every combination of discrete x, t coordinates.

The kernels $\underline{\mathbf{H}}$ are $(N_xN_t) \times N_{v_x}$ or $(N_xN_t) \times N_{v_t}$ matrices, where N_x, N_t and N_{v_x}, N_{v_t} are the number of grid points in the x, t and v_x, v_t dimensions. The $\boldsymbol{p}$ and $\boldsymbol{r}$ are $N_{v_x} \times 1$ or $N_{v_t} \times 1$ vectors, and $\boldsymbol{U}$—the stochastic field realization—is an $(N_xN_t) \times 1$ vector, which must be reshaped to an $N_x \times N_t$ matrix. The $\boldsymbol{r}$ are vectors of standard complex normal random numbers.

In these simulations, $N_x = N_t = N_{v_x} = N_{v_t} = 512, \Delta v_x = (N_x\Delta x)^{-1} = 72.7\,\text{m}^{-1}$, and $\Delta v_t = (N_t\Delta t)^{-1} = 1.76$ GHz. Likewise, for the space-frequency source simulations, $N_x = N_\omega = N_{v_x} = N_{v_\omega} = 512$, $\Delta v_x = (N_x\Delta x)^{-1} = 72.7\ \text{m}^{-1}$, and $\Delta v_\omega = (N_\omega\Delta\omega)^{-1} = 1.76$ ps. Table 1 lists the parameter values for the simulated twisted space-frequency and space-time GSM partially coherent beams.

λ_c	1 μm
W_x	0.5 mm
δ_x	0.269 mm
W_ω, W_t	70.7 GHz, 70.7 ps
δ_ω, δ_t	33.3 GHz, 33.3 ps
μ	0.10 (mm GHz)$^{-1}$, 0.10 (mm ps)$^{-1}$
σ_x	11 mm^{-2}
σ_ω, σ_t	700 THz^{-2}, 700 ns^{-2}
α	0.13 mm^2
β	0.002 THz^2; 0.002 ns^2

Table 1. Simulated twisted space-frequency and space-time GSM beam parameters.

After generating a field instance using Eq. (17) and the values listed in Table 1, we digitally propagated U $z = 0.126$ m, 0.262 m, 0.524 m, 1.05 m, 3.14 m, and 6.28 m—corresponding to Fresnel numbers $N_F = 25$, 12, 6, 3, 1, and 0.5, respectively. For the twisted space-frequency field instances, we performed the propagations by evaluating the Fresnel integral along the x dimension of each realization U using a fast Fourier transform (FFT)[46,47]. The process was slightly different for the twisted space-time field realizations. We first transformed the twisted space-time field instance U to the x-ω domain using a FFT computed along the t dimension of U. We then propagated that field using the Fresnel integral (again, evaluated using a FFT) computed along the x dimension of U. Lastly, we transformed the field back to the x-t domain using a FFT computed along the ω dimension of U.

From 5,000 propagated field realizations of twisted space-frequency and space-time GSM partially coherent beams, we computed the sample spectral densities S and mean intensities I, respectively. In addition, we computed planar slices through the four-dimensional CSDs W and MCFs Γ, respectively.

In the next section, we compare these sample moments to their corresponding theoretical quantities derived and discussed earlier in the paper. The purpose of this is twofold: to verify that we have indeed produced the desired twisted space-frequency or space-time GSM source, and to validate our theory presented in the prior section.

We have included the MATLAB R2018b scripts (.m files) required to execute these wave-optics simulations as Supplementary Code C1.

Results. Because the behaviors of the twisted space-frequency and space-time GSM sources simulated here are identical in their respective domains (x-ω in the former, x-t in the latter), we present results for both that are complementary, such that the spectral density S and mean intensity I, and CSD W and MCF Γ are presented for all N_F, but not duplicated.

We begin with the S and I results, which are shown in Figs. 2 and 3, respectively. The layout of the figures is identical. Proceeding down the rows, the S or I are displayed for a particular N_F. The Fresnel numbers are annotated on the figures for the reader's convenience. Proceeding from left to right across the columns are the theoretical and simulated two-dimensional S or I in columns 1 and 2, respectively. The theoretical and simulated S or I images use the same false color scales defined by the color bars immediately following column 2. The last two columns report the one-dimensional profiles or slices through the theoretical and simulated (labeled "Thy" and "Sim" in the legends) S or I, plotted on the same axes for ease of comparison. Column 3 shows the ω or t slices, and column 4 displays the x slices.

The agreement between theory and simulation is excellent. The quality of these results imply that we have successfully generated twisted space-frequency and space-time sources that radiate the desired S and I. While these results are certainly positive, we still must verify that we have generated twisted space-frequency and space-time beams with the desired coherence properties. This requires examination of the cross-spectral density and mutual coherence functions, respectively.

Figures 4 and 5 show $W(x_1, 0, \omega_c, \omega_2, z)$ and $\Gamma(x_1, 0, z/c, t_2, z)$. We removed the piston phase shifts, $\exp\left[\mathrm{j}(k_1 - k_2)z\right]$ and $\exp\left[-\mathrm{j}\omega_c(t_1 - t_2)\right]$, from these results. Both figures consist of three groups of four images. Each image group corresponds to an N_F, labeled for the reader's convenience. Inside each group, the four images are arranged in two rows and two columns. The first column presents the theoretical W or Γ, while the second column displays the simulated results. The first row shows the real parts of W or Γ; the second row shows the imaginary parts. The theoretical and simulated W or Γ use the same false color scales defined by the color bars at rows' end.

Again, the agreement between theory and simulation is excellent. The quality of these results, in combination with those in Figs. 2 and 3, prove that we have indeed generated twisted space-frequency and space-time GSM beams with the parameters given in Table 1.

Physical synthesis. Before concluding, it is worth discussing how to physically synthesize these partially coherent beams. Here, we focus on twisted space-time GSM partially coherent sources, as the setup to synthesize twisted space-frequency GSM beams is similar.

Figure 6 shows a schematic of an optical system that can be used to synthesize a twisted space-time partially coherent source. This device is known as a Fourier transform pulse shaper[23,26,48–51].

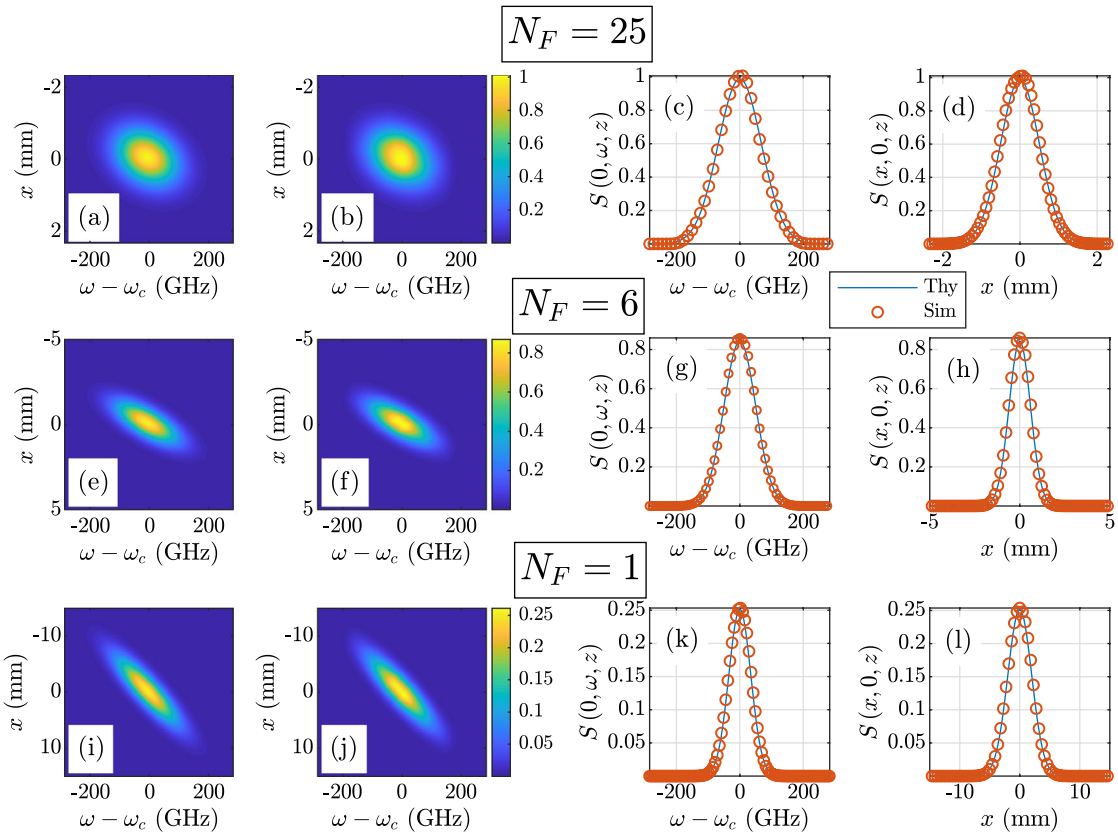

Figure 2. Twisted space-frequency GSM spectral density $S(x, \omega, z)$ results. The theoretical spectral density S^{thy} is given in Eq. (8): $N_F = 25$—(**a**) S^{thy}, (**b**) S^{sim}, (**c**) $S(0, \omega, z)$ theory versus simulation, and (**d**) $S(x, 0, z)$ theory versus simulation; $N_F = 6$—(**e**) S^{thy}, (**f**) S^{sim}, (**g**) $S(0, \omega, z)$ theory versus simulation, and (**h**) $S(x, 0, z)$ theory versus simulation; $N_F = 1$—(**i**) S^{thy}, (**j**) S^{sim}, (**k**) $S(0, \omega, z)$ theory versus simulation, and (**l**) $S(x, 0, z)$ theory versus simulation.

We assume a coherent Gaussian pulse as the input field into the shaper, i.e.,

$$U^{\text{in}}(x, t) = \exp\left(-\frac{x^2}{4W_x^2}\right) \exp\left(-\frac{t^2}{4W_t^2}\right) \exp\left(-\text{j}\omega_c t\right). \tag{18}$$

This field is incident on a grating (G), which in combination with a cylindrical lens (CL) of focal length f, maps the spectrum of U^{in} into physical space at the plane of the spatial light modulator (SLM). The SLM modifies the field in the x-ω domain, introducing random space-frequency coupling. The field then transits another cylindrical lens (of focal length f) and an identical grating to the first. This combination reverses the spectrum-to-space mapping of the first G-CL system, resulting in a stochastic fully-coherent realization of a twisted space-time GSM partially coherent beam (U^{out} in the figure). Partial coherence is introduced by incoherently summing many such realizations, or pulses. Although we have ignored it for mathematical convenience, we note that the spatial distribution of the beam in the y direction is generally unaffected by the pulse shaper[27]. The beam, therefore, can be spatially shaped either before or after the pulse shaper.

In contrast to the simulations and, in particular, Eqs. (16) and (17), the SLM in Fig. 6, which produces the field realization, operates in the x-ω plane. Therefore, the kernel H in Eq. (10) must be transformed into that domain, namely,

$$\begin{aligned}
H(x, \omega; \nu_x, \nu_t) &= \frac{1}{2\pi} \int_{-\infty}^{\infty} H(x, t; \nu_x, \nu_t) \exp\left(\text{j}\omega t\right) \text{d}t = H(x, \omega; \nu_x) H(x, \omega; \nu_t) \\
H(x, \omega; \nu_x) &= \sqrt{\frac{1}{2\sqrt{\pi\sigma_t}}} \exp\left(-\frac{\sigma_x}{2} x^2\right) \exp\left(-\frac{\bar{\omega}^2}{8\sigma_t}\right) \exp\left(\frac{\alpha^2\mu^2}{4\sigma_t} \nu_x^2\right) \exp\left[-\text{j}\left(x + \frac{\alpha\mu}{2\sigma_t}\bar{\omega}\right)\nu_x\right] \\
H(x, \omega; \nu_t) &= \sqrt{\frac{1}{2\sqrt{\pi\sigma_t}}} \exp\left(-\frac{\sigma_x}{2} x^2\right) \exp\left(-\frac{\bar{\omega}^2}{8\sigma_t}\right) \exp\left(-\frac{\nu_t^2}{4\sigma_t}\right) \exp\left[\left(\beta\mu x + \frac{1}{2\sigma_t}\bar{\omega}\right)\nu_t\right].
\end{aligned} \tag{19}$$

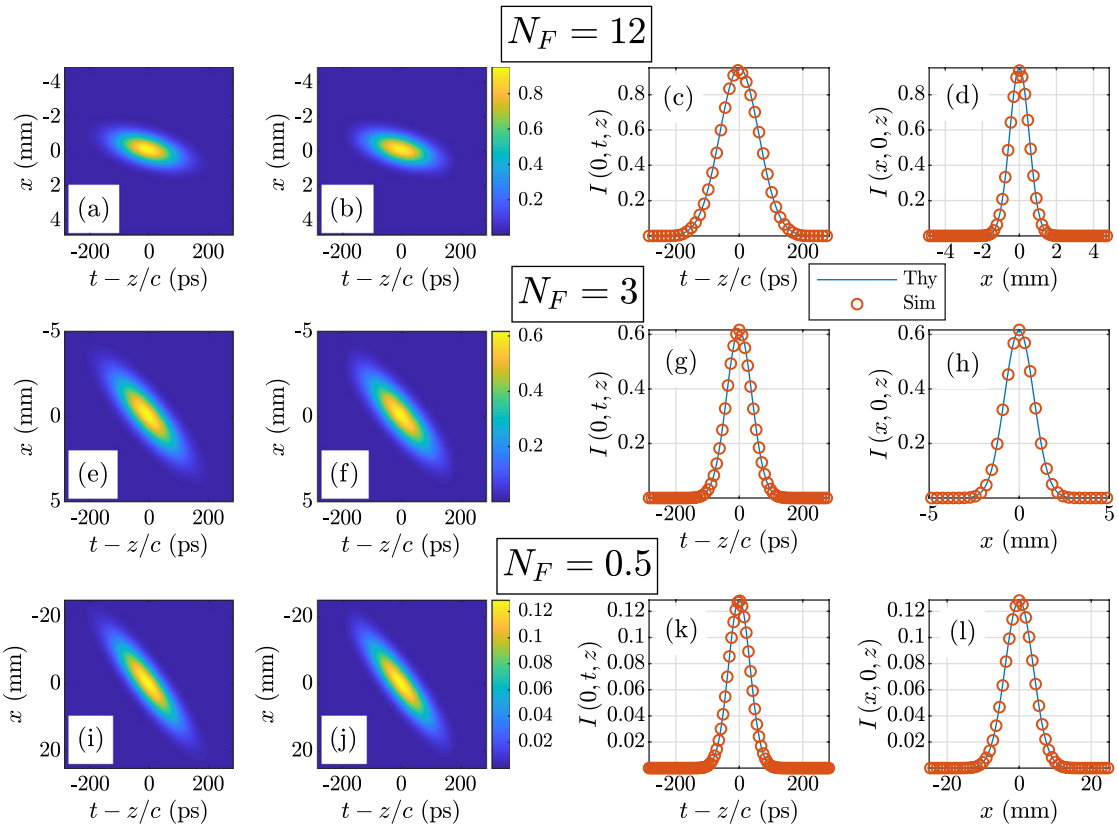

Figure 3. Twisted space-time GSM mean intensity $I(x,t,z)$ results. The theoretical mean intensity I^{thy} is given in Eq. (15): $N_F = 12$—(**a**) I^{thy}, (**b**) I^{sim}, (**c**) $I(0,t,z)$ theory versus simulation, and (**d**) $I(x,0,z)$ theory versus simulation; $N_F = 3$—(**e**) I^{thy}, (**f**) I^{sim}, (**g**) $I(0,t,z)$ theory versus simulation, and (**h**) $I(x,0,z)$ theory versus simulation; $N_F = 0.5$—(**i**) I^{thy}, (**j**) I^{sim}, (**k**) $I(0,t,z)$ theory versus simulation, and (**l**) $I(x,0,z)$ theory versus simulation.

The coefficients for $H(x,\omega;v_x)$ and $H(x,\omega;v_t)$ are included for completeness. They scale the on-axis intensity of the beam and can be neglected. The kernel $H(x,\omega;v_x)$ grows without bound because of the v_x exponential; however, when multiplied by $\sqrt{p(v_x)}$, the superposition integral [see Eq. (16)] converges.

We close this section with a brief discussion of hardware considerations for the apparatus in Fig. 6. Note that additional information can be found in Refs.[23,26,48–51] and the references cited therein. The most critical component in Fig. 6 is the SLM, which ideally, should cycle at the source's pulse repetition frequency. This ensures that every pulse is statistically independent of every other pulse and therefore, quick convergence to the desired twisted space-time partially coherent beam.

SLM speed depends heavily on type, e.g., liquid-crystal SLMs have refresh rates of 100s of Hz, segmented deformable mirrors (DMs) and digital micromirror devices (DMDs) refresh at rates of 10s of kHz. Of course, speed is not the only consideration. Liquid-crystal SLMs can have millions of pixels—orders of magnitude more than segmented DMs—and are more light efficient than DMDs, which are binary devices. More information on these SLMs can be found in Refs.[52–59]. As mentioned in Ref.[51], since the MCF (or CSD) is computed over the ensemble of all possible field, or pulse realizations, SLM speed does not matter if the goal is solely to produce the partially coherent source. Although obvious, SLM choice ultimately depends on the application.

Conclusion

In this paper, we presented space-frequency and space-time extensions to Simon and Mukunda's spatially twisted partially coherent beams. Like the recently introduced STOV fields, which provided the impetus for this work, twisted space-frequency and space-time partially coherent beams possess transverse OAM.

Starting with the superposition rule for genuine partially coherent sources, we derived the CSD and MCF for twisted space-frequency and space-time partially coherent sources, respectively. Assuming a GSM form for the twisted sources, we examined their free-space propagation behaviors by evaluating the paraxial CSD and MCF propagation integrals. We derived expressions for the spectral density and mean intensity for any plane $z > 0$ and described both physically.

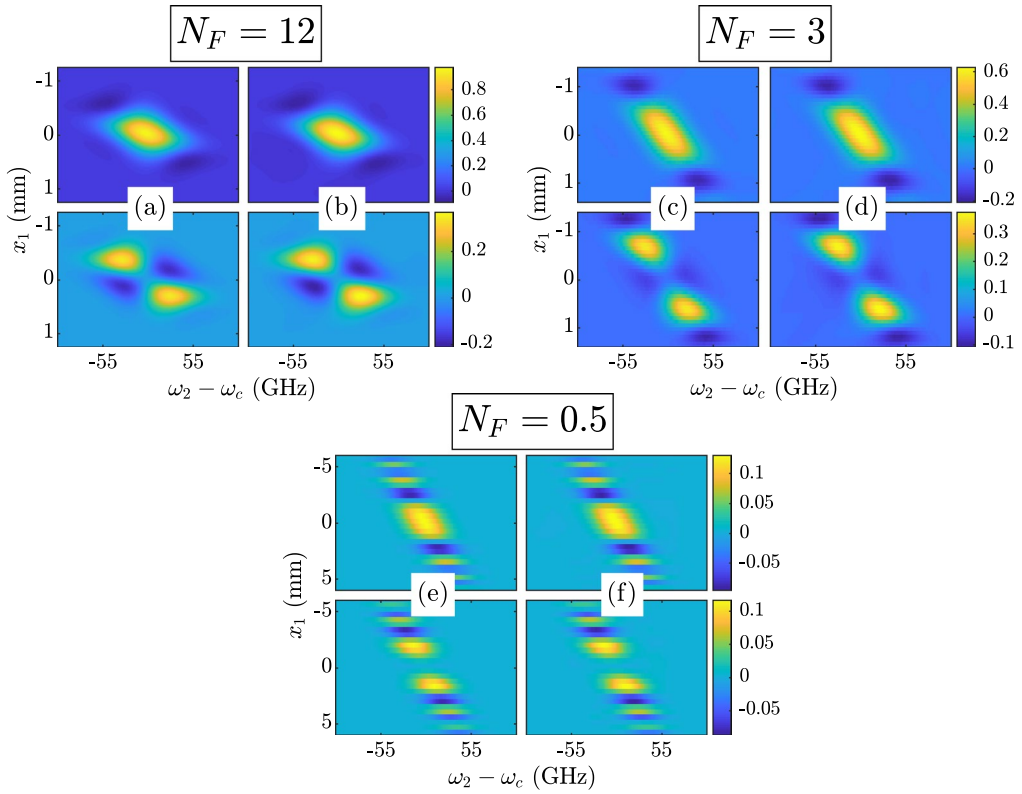

Figure 4. Twisted space-frequency GSM $W(x_1, 0, \omega_c, \omega_2, z)$ results. The theoretical CSD W^{thy} is given in Eq. (7): $N_F = 12$—(**a**) top $\text{Re}\left(W^{\text{thy}}\right)$, bottom $\text{Im}\left(W^{\text{thy}}\right)$ and (**b**) top $\text{Re}\left(W^{\text{sim}}\right)$, bottom $\text{Im}\left(W^{\text{sim}}\right)$; $N_F = 3$ —(**c**) top $\text{Re}\left(W^{\text{thy}}\right)$, bottom $\text{Im}\left(W^{\text{thy}}\right)$ and (**d**) top $\text{Re}\left(W^{\text{sim}}\right)$, bottom $\text{Im}\left(W^{\text{sim}}\right)$; $N_F = 0.5$—(**e**) top $\text{Re}\left(W^{\text{thy}}\right)$, bottom $\text{Im}\left(W^{\text{thy}}\right)$ and (**f**) top $\text{Re}\left(W^{\text{sim}}\right)$, bottom $\text{Im}\left(W^{\text{sim}}\right)$.

To validate our work, we simulated the generation and propagation of example twisted space-frequency and space-time partially coherent beams. We described the details of our simulations and the stochastic field realization process. We compared the simulated, or sample second-order field moments—spectral densities, mean intensities, CSDs, and MCFs—to their corresponding theoretical expressions. The simulated and theoretical moments were found to be in excellent agreement.

Lastly, we described how to physically generate stochastic realizations of these beams using a device known as a Fourier transform pulse shaper, which consisted of two identical gratings, cylindrical lenses, and a SLM. We briefly discussed the characteristics of different types of SLMs, and the pros and cons of using them in the shaper to generate random pulse realizations.

Light that possesses transverse angular momentum is a relatively recent phenomenon and an exciting new area of beam control research. Considering the applications which use traditional, spatially twisted or vortex light[3–8,10–21], we should expect that space-frequency or space-time twisted beams (including STOVs) will be used in optical tweezing, particle manipulation, optical communications, and astronomy in novel ways[24,26,60]. In addition, there has been recent work in coupling spin (concerns circular polarization) and orbital angular momenta resulting in novel light control, generation, and optical manipulation techniques[61–63]. Similar coupling is possible with space-frequency and space-time twisted partially coherent beams by generalizing the scalar analysis presented in this paper to include the vector or electromagnetic nature of these stochastic light sources. The work we present here adds to the exciting new field of light beams carrying transverse angular momentum as well as the existing, rich literature on partially coherent sources.

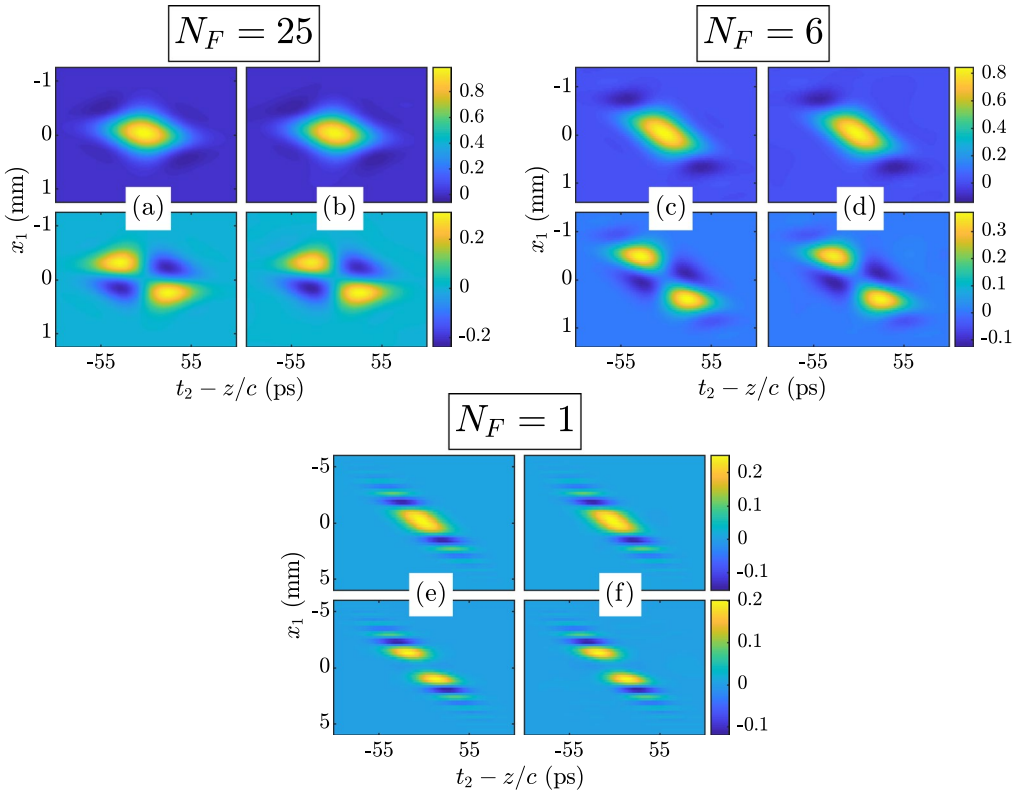

Figure 5. Twisted space-time GSM $\Gamma(x_1, 0, z/c, t_2, z)$ results. The theoretical MCF Γ^{thy} is given in Eq. (13): $N_F = 25$—(**a**) top $\text{Re}\left(\Gamma^{\text{thy}}\right)$, bottom $\text{Im}\left(\Gamma^{\text{thy}}\right)$ and (**b**) top $\text{Re}\left(\Gamma^{\text{sim}}\right)$, bottom $\text{Im}\left(\Gamma^{\text{sim}}\right)$; $N_F = 6$—(**c**) top $\text{Re}\left(\Gamma^{\text{thy}}\right)$, bottom $\text{Im}\left(\Gamma^{\text{thy}}\right)$ and (**d**) top $\text{Re}\left(\Gamma^{\text{sim}}\right)$, bottom $\text{Im}\left(\Gamma^{\text{sim}}\right)$; $N_F = 1$—(**e**) top $\text{Re}\left(\Gamma^{\text{thy}}\right)$, bottom $\text{Im}\left(\Gamma^{\text{thy}}\right)$ and (**f**) top $\text{Re}\left(\Gamma^{\text{sim}}\right)$, bottom $\text{Im}\left(\Gamma^{\text{sim}}\right)$.

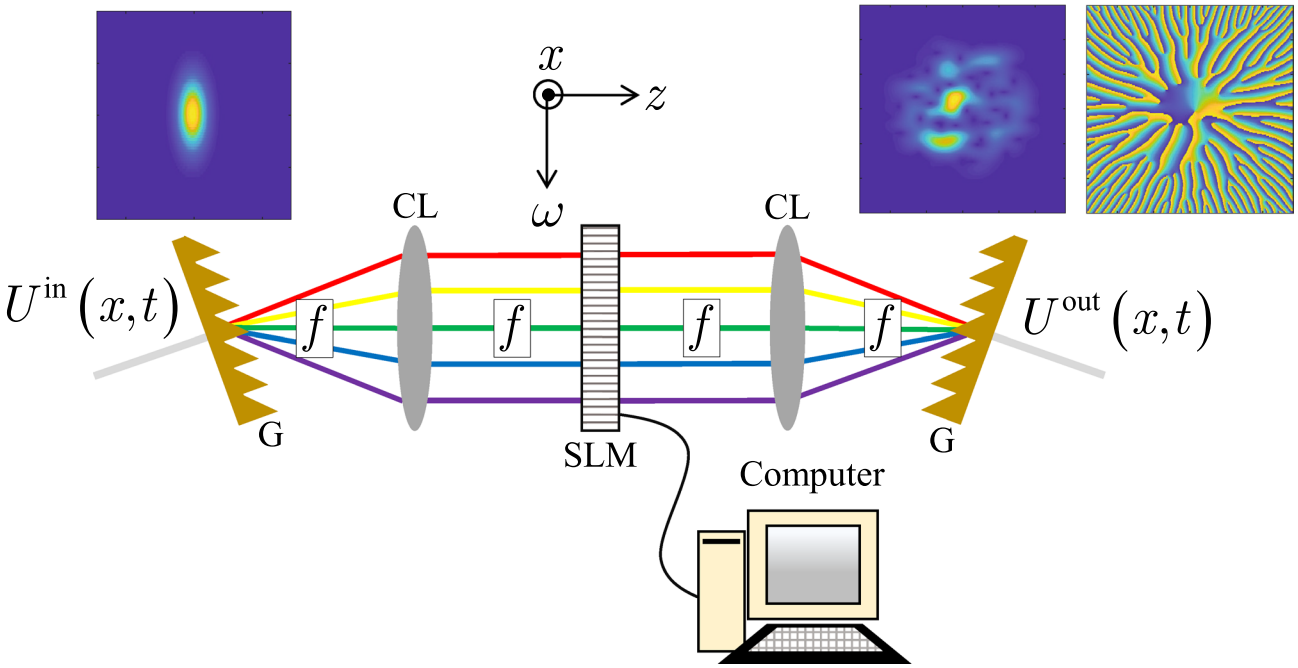

Figure 6. Fourier transform pulse shaper—G is grating, CL is cylindrical lens, and SLM is spatial light modulator.

Received: 9 May 2020; Accepted: 26 June 2020
Published online: 24 July 2020

References

1. Allen, L., Beijersbergen, M. W., Spreeuw, R. J. C. & Woerdman, J. P. Orbital angular momentum of light and the transformation of Laguerre-Gaussian laser modes. *Phys. Rev. A***45**, 8185–8189. https://doi.org/10.1103/PhysRevA.45.8185 (1992).
2. Allen, L., Padgett, M. & Babiker, M. The orbital angular momentum of light. In Wolf, E. (ed.) *Prog. Opt.*, vol. 39 of *Prog. Opt.*, chap. 4, 291–372, https://doi.org/10.1016/S0079-6638(08)70391-3 (Elsevier, Amsterdam, 1999).
3. Gao, D. *et al.* Optical manipulation from the microscale to the nanoscale: fundamentals, advances and prospects. *Light. Sci. Appl.***6**, e17039. https://doi.org/10.1038/lsa.2017.39 (2017).
4. Yao, A. M. & Padgett, M. J. Orbital angular momentum: origins, behavior and applications. *Adv. Opt. Photon.***3**, 161–204. https://doi.org/10.1364/AOP.3.000161 (2011).
5. Padgett, M. & Bowman, R. Tweezers with a twist. *Nat. Photon.***5**, 343 (2011).
6. Gbur, G. J. *Singular Optics* (CRC, Boca Raton, FL, 2016).
7. Padgett, M. J. Orbital angular momentum 25 years on. *Opt. Express***25**, 11265–11274. https://doi.org/10.1364/OE.25.011265 (2017).
8. Shen, Y. *et al.* Optical vortices 30 years on: OAM manipulation from topological charge to multiple singularities. *Light Sci. Appl.***8**, 90 (2019).
9. Simon, R. & Mukunda, N. Twisted Gaussian Schell-model beams. *J. Opt. Soc. Am. A***10**, 95–109. https://doi.org/10.1364/JOSAA.10.000095 (1993).
10. Ambrosini, D., Bagini, V., Gori, F. & Santarsiero, M. Twisted Gaussian Schell-model beams: a superposition model. *J. Mod. Opt.***41**, 1391–1399. https://doi.org/10.1080/09500349414551331 (1994).
11. Friberg, A. T., Tervonen, E. & Turunen, J. Interpretation and experimental demonstration of twisted Gaussian Schell-model beams. *J. Opt. Soc. Am. A***11**, 1818–1826. https://doi.org/10.1364/JOSAA.11.001818 (1994).
12. Gori, F., Santarsiero, M., Borghi, R. & Vicalvi, S. Partially coherent sources with helicoidal modes. *J. Mod. Opt.***45**, 539–554. https://doi.org/10.1080/09500349808231913 (1998).
13. Ponomarenko, S. A. Twisted Gaussian Schell-model solitons. *Phys. Rev. E***64**, 036618. https://doi.org/10.1103/PhysRevE.64.036618 (2001).
14. Mei, Z. & Korotkova, O. Random sources for rotating spectral densities. *Opt. Lett.***42**, 255–258. https://doi.org/10.1364/OL.42.000255 (2017).
15. Stahl, C. S. D. & Gbur, G. Twisted vortex Gaussian Schell-model beams. *J. Opt. Soc. Am. A***35**, 1899–1906. https://doi.org/10.1364/JOSAA.35.001899 (2018).
16. Gori, F. & Santarsiero, M. Devising genuine twisted cross-spectral densities. *Opt. Lett.***43**, 595–598. https://doi.org/10.1364/OL.43.000595 (2018).
17. Borghi, R. Twisting partially coherent light. *Opt. Lett.***43**, 1627–1630. https://doi.org/10.1364/OL.43.001627 (2018).
18. Wan, L. & Zhao, D. Controllable rotating Gaussian Schell-model beams. *Opt. Lett.***44**, 735–738. https://doi.org/10.1364/OL.44.000735 (2019).
19. Wan, L. & Zhao, D. Generalized partially coherent beams with nonseparable phases. *Opt. Lett.***44**, 4714–4717. https://doi.org/10.1364/OL.44.004714 (2019).
20. Wang, H. *et al.* Generating bona fide twisted Gaussian Schell-model beams. *Opt. Lett.***44**, 3709–3712. https://doi.org/10.1364/OL.44.003709 (2019).
21. Santarsiero, M., Gori, F. & Alonzo, M. Higher-order twisted/astigmatic Gaussian Schell-model cross-spectral densities and their separability features. *Opt. Express***27**, 8554–8565. https://doi.org/10.1364/OE.27.008554 (2019).
22. Sukhorukov, A. P. & Yangirova, V. V. Spatio-temporal vortices: properties, generation and recording. *Proc. SPIE***5949**, 35–43. https://doi.org/10.1117/12.623906 (2005).
23. Dallaire, M., McCarthy, N. & Piché, M. Spatiotemporal Bessel beams: theory and experiments. *Opt. Express***17**, 18148–18164. https://doi.org/10.1364/OE.17.018148 (2009).
24. Bliokh, K. Y. & Nori, F. Spatiotemporal vortex beams and angular momentum. *Phys. Rev. A***86**, 033824. https://doi.org/10.1103/PhysRevA.86.033824 (2012).
25. Jhajj, N. *et al.* Spatiotemporal optical vortices. *Phys. Rev. X***6**, 031037. https://doi.org/10.1103/PhysRevX.6.031037 (2016).
26. Chong, A., Wan, C., Chen, J. & Zhan, Q. Generation of spatiotemporal optical vortices with controllable transverse orbital angular momentum. *Nat. Photon.* (2020).
27. Hancock, S. W., Zahedpour, S., Goffin, A. & Milchberg, H. M. Free-space propagation of spatiotemporal optical vortices. *Optica***6**, 1547–1553. https://doi.org/10.1364/OPTICA.6.001547 (2019).
28. Akturk, S., Gu, X., Gabolde, P. & Trebino, R. The general theory of first-order spatio-temporal distortions of Gaussian pulses and beams. *Opt. Express***13**, 8642–8661. https://doi.org/10.1364/OPEX.13.008642 (2005).
29. Wang, L., Lin, Q., Chen, H. & Zhu, S. Propagation of partially coherent pulsed beams in the spatiotemporal domain. *Phys. Rev. E***67**, 056613. https://doi.org/10.1103/PhysRevE.67.056613 (2003).
30. Mandel, L. & Wolf, E. *Optical Coherence and Quantum Optics* (Cambridge University, New York, 1995).
31. Korotkova, O. *Random Light Beams: Theory and Applications* (CRC, Boca Raton, FL, 2014).
32. Gori, F. & Santarsiero, M. Devising genuine spatial correlation functions. *Opt. Lett.***32**, 3531–3533. https://doi.org/10.1364/OL.32.003531 (2007).
33. Martínez-Herrero, R., Mejías, P. M. & Gori, F. Genuine cross-spectral densities and pseudo-modal expansions. *Opt. Lett.***34**, 1399–1401. https://doi.org/10.1364/OL.34.001399 (2009).
34. Korotkova, O. Random sources for rectangular far fields. *Opt. Lett.***39**, 64–67. https://doi.org/10.1364/OL.39.000064 (2014).
35. Simon, R. & Mukunda, N. Twist phase in Gaussian-beam optics. *J. Opt. Soc. Am. A***15**, 2373–2382. https://doi.org/10.1364/JOSAA.15.002373 (1998).
36. Lin, Q. & Cai, Y. Tensor ABCD law for partially coherent twisted anisotropic Gaussian-Schell model beams. *Opt. Lett.***27**, 216–218. https://doi.org/10.1364/OL.27.000216 (2002).
37. Charnotskii, M. Transverse linear and orbital angular momenta of beam waves and propagation in random media. *J. Opt.***20**, 025602 (2018).
38. Razueva, E. & Abramochkin, E. Multiple-twisted spiral beams. *J. Opt. Soc. Am. A***36**, 1089–1097. https://doi.org/10.1364/JOSAA.36.001089 (2019).
39. Rego, L. *et al.* Generation of extreme-ultraviolet beams with time-varying orbital angular momentum. *Science***364**, https://doi.org/10.1126/science.aaw9486 (2019).
40. Lajunen, H., Vahimaa, P. & Tervo, J. Theory of spatially and spectrally partially coherent pulses. *J. Opt. Soc. Am. A***22**, 1536–1545 (2005).
41. Christov, I. Propagation of partially coherent light pulses. *Opt. Acta***33**, 63–72, https://doi.org/10.1080/713821858 (1986).
42. Lancis, J., Torres-Company, V., Silvestre, E. & Andrés, P. space–time analogy for partially coherent plane-wave-type pulses. *Opt. Lett.***30**, 2973–2975 (2005).

43. Yao, M., Cai, Y., Korotkova, O., Lin, Q. & Wang, Z. Spatio-temporal coupling of random electromagnetic pulses interacting with reflecting gratings. *Opt. Express***18**, 22503–22514. https://doi.org/10.1364/OE.18.022503 (2010).
44. Lin, Q., Wang, L. & Zhu, S. Partially coherent light pulse and its propagation. *Opt. Commun.***219**, 65–70. https://doi.org/10.1016/S0030-4018(03)01340-3 (2003).
45. Hyde, M. W. Stochastic complex transmittance screens for synthesizing general partially coherent sources. *J. Opt. Soc. Am. A***37**, 257–264. https://doi.org/10.1364/JOSAA.381772 (2020).
46. Schmidt, J. D. *Numerical Simulation of Optical Wave Propagation with Examples in MATLAB* (SPIE Press, Bellingham, WA, 2010).
47. Voelz, D. G. *Computational Fourier Optics: A MATLAB Tutorial* (SPIE, Bellingham, WA, 2011).
48. Weiner, A. M. Femtosecond pulse shaping using spatial light modulators. *Rev. Sci. Instrum.***71**, 1929–1960. https://doi.org/10.1063/1.1150614 (2000).
49. Kondakci, H. E. & Abouraddy, A. F. Diffraction-free space–time light sheets. *Nat. Photon.***11**, 733–740 (2017).
50. Torres-Company, V., Lancis, J. & Andrés, P. space–time analogies in optics. In Wolf, E. (ed.) *Prog. Opt.*, vol. 56 of *Prog. Opt.*, chap. 1, 1–80, https://doi.org/10.1016/B978-0-444-53886-4.00001-0 (Elsevier, Amsterdam, 2011).
51. Ding, C., Koivurova, M., Turunen, J., Setälä, T. & Friberg, A. T. Coherence control of pulse trains by spectral phase modulation. *J. Opt.***19**, 095501 (2017).
52. Gmuender, T. *DLP Using Digital Micromirror Devices: A Primer* (SPIE Press, Bellingham, WA, 2016).
53. Stilgoe, A. B., Kashchuk, A. V., Preece, D. & Rubinsztein-Dunlop, H. An interpretation and guide to single-pass beam shaping methods using SLMs and DMDs. *J. Opt.***18**, 065609 (2016).
54. Scholes, S., Kara, R., Pinnell, J., Rodríguez-Fajardo, V. & Forbes, A. Structured light with digital micromirror devices: a guide to best practice. *Opt. Eng.***59**, 1–12. https://doi.org/10.1117/1.OE.59.4.041202 (2019).
55. Hyde, M. W., Bose-Pillai, S. R. & Wood, R. A. Synthesis of non-uniformly correlated partially coherent sources using a deformable mirror. *Appl. Phys. Lett.***111**, 101106. https://doi.org/10.1063/1.4994669 (2017).
56. Zhang, Z., You, Z. & Chu, D. Fundamentals of phase-only liquid crystal on silicon (LCOS) devices. *Light Sci. Appl.***3**, e213. https://doi.org/10.1038/lsa.2014.94 (2014).
57. Yu, X., Todi, A. & Tang, H. Bessel beam generation using a segmented deformable mirror. *Appl. Opt.***57**, 4677–4682. https://doi.org/10.1364/AO.57.004677 (2018).
58. Rosales-Guzmán, C. & Forbes, A. *How to Shape Light with Spatial Light Modulators* (SPIE Press, Bellingham, WA, 2017).
59. Lazarev, G., Hermerschmidt, A., Krüger, S. & Osten, S. LCOS spatial light modulators: Trends and applications. In Osten, W. & Reingand, N. (eds.) *Optical Imaging and Metrology: Advanced Technologies*, chap. 1, 1–29 (Wiley-Blackwell, 2012).
60. Lin, K. *et al.* Spatiotemporal rotational dynamics of laser-driven molecules. *Adv. Photonics***2**, 1–21. https://doi.org/10.1117/1.AP.2.2.024002 (2020).
61. Cardano, F. & Marrucci, L. Spin-orbit photonics. *Nat. Photonics***9**, 776–778 (2015).
62. Bliokh, K. Y., Rodríguez-Fortuño, F. J., Nori, F. & Zayats, A. V. Spin-orbit interactions of light. *Nat. Photonics***9**, 796–808 (2015).
63. Aiello, A., Banzer, P., Neugebauer, M. & Leuchs, G. From transverse angular momentum to photonic wheels. *Nat. Photon.***9**, 789–795 (2015).

Acknowledgements

The views expressed in this paper are those of the authors and do not reflect the official policy or position of the U.S. Air Force, the Department of Defense, or the U.S. Government. I would like to thank Professor Olga Korotkova for reviewing and providing feedback on this paper.

Author contributions

M.W.H. performed the works of conceptualization, formal analysis, methodology, software, validation, visualization, writing—original draft, reviewing, and editing.

Competing interests

The author declares no competing interests.

Additional information

Supplementary information is available for this paper at https://doi.org/10.1038/s41598-020-68705-9.

Correspondence and requests for materials should be addressed to M.W.H.

Reprints and permissions information is available at www.nature.com/reprints.

Publisher's note Springer Nature remains neutral with regard to jurisdictional claims in published maps and institutional affiliations.